XVII[th] World Congress of the International Commission of Agricultural and Biosystems Engineering (CIGR)

Hosted by the Canadian Society for Bioengineering (CSBE/SCGAB)
Québec City, Canada June 13-17, 2010

HOW TO INTEGRATE MULTI-SENSOR DATA FOR PRECISION AGRICULTURE

A. CASTRIGNANÒ[1], M T F WONG[2], D. DE BENEDETTO[1] AND D. SOLLITTO[1]

[1]A. CASTRIGNANÒ, CRA-SCA via Celso Ulpiani, 5. Bari-Italy, annamaria.castrignano@entecra.it
[2]M T F WONG, CSIRO Land and Water, Wembley, Western Australia WA 6014, mike.wong@csiro.au

CSBE101306– Presented at Section 1: Land and Water Engineering Conference

ABSTRACT Geo-electrical sensors are often used as auxiliary variables with sparse direct measurements to estimate soil properties. Using a single sensor often proved problematic, but use of complementary sensors can compensate such weaknesses. The objective of this work was to integrate field data from EMI (EM38, EM31), γ-ray and DGPS sensors for delineating areas of homogeneous soil. The geophysical survey was carried out on an 80-ha cropping field in Corrigin, Western Australia. The EM38 and EM31 data were strongly correlated between them as were γ-radiometric counts from thorium (Th), uranium (U) and all elements (Tc). The multi-sensor data were split into 4 subgroups, based on their similarities: 1) EMI data; 2) γ-radiometric counts from potassium (K); 3) γ-radiometric counts from Th, U and Tc and 4) DGPS height. Each group of data was separately analysed using geostatistical techniques. The EMI data showed anisotropy and an anisotropic Linear Model of Coregionalisation was used before cokriging. The EM31 and EM38 maps looked similar. The maps of γ-U, Th and Tc were also similar, suggesting that they reflected the same soil properties, but were somewhat different form the γ-K maps. High values of EMI coincided with both low γ-radiometric values at the valley bottom, due to moist sandy salinity-prone soil of varying depth to texture contrast, and high γ-radiometric values at elevated areas of the field due to emission from finer textured soil. High γ-radiometric values coincided with low values of EMI over gravelly sands. Only the use of a multi-sensor platform could discriminate soils that gave similar outputs to one sensor. The first two Principal Components of the geophysical data were used to partition the field into homogeneous areas.

Keywords: EMI sensor, gamma emission, DGPS, geostatistics, Management zone

INTRODUCTION

Spatially detailed data from electromagnetic induction (EMI) sensors are often used as auxiliary variables with sparse direct measurements to estimate soil properties at high spatial resolutions matching those of yield maps (McBratney et al., 2005, Wong and Asseng, 2006). Such high-resolution soil property maps, combined with process models, have allowed the causes of spatial and seasonal variations in wheat yield to be determined to support management (Wong and Asseng, 2006). This approach also allowed field locations prone to deep drainage and nitrate leaching to be identified for targeted management (Wong et al., 2006).

EMI sensing responds to temperature, clay content, mineralogy, moisture content and bulk density (McBratney et al., 2005). It has been used to estimate soil depth to underlying clayey hardpan (Doolittle et al., 1994) and salinity (Kaffka et al., 2005). Occurrence of salt in dryland and coastal environments is a common interference in the estimation of soil properties (other than salinity), but EMI sensing is unable to discriminate clay soils from saline soils because both result in high values of bulk electrical conductivity. An additional weakness of EMI methods is inability to distinguish between sandy soils and gravels because these materials give similar low values. Soil depth and hence depth-limited plant available water content (PAWC) therefore cannot be estimated in landscapes with shallow soils over gravels (Wong et al., 2009) from EMI sensor outputs. Such shortcomings can be overcome by complementing EMI methods with other sensors that are not subject to the same weaknesses.

Gamma ray spectrometry is a relatively new soil sensing technique that can be carried out from either ground or airborne platforms. The spectrometer measures natural γ-emissions from emitters such as 40K, the daughter radionuclides of 238U and 232Th and total emission from all elements. Association of these radionuclides with clay, gravels, and soil-forming materials led to variations in the concentrations of these emitters to be used to estimate soil properties such as clay, potassium, organic carbon and iron contents, soil depth, and soil pH (Viscarra Rossel et al., 2007, Wong et al., 2008). Ambiguity in the interpretation of radiometric data arises when soils with varying gravel and clay contents occur across the surveyed area as they both give rise to strong signals. This problem is not encountered with EMI, since clays and gravels give rise to markedly different EMI values.

To optimize the use of soil and water resources and increase farmer profitability and environment protection, we need management practices to take account of variable site conditions. This is the main objective of Precision Agriculture. Recent research has focused on use of Management Zones (MZ) that are defined as subfield regions or classes within which the effects on the crop of seasonal differences in weather, soil, topography, management, etc are expected to be more or less uniform (Lark, 1998). Determination of these sub-field areas is difficult due to the interactions among several biotic, abiotic and climate factors that affect crop yield and different approaches have been developed for delination of site-specific management zones. A very promising non-invasive approach to define the boundaries of MZ involves the use of electromagnetic induction to measure bulk electrical conductivity (EC_a). This approach has been used to effectively map variations in surface soil properties such as salinity, water content and clay (Corwin and Lesch, 2003; Kitchen et al, 2003). Castrignanò et al., 2006 and Morari et al., 2009 showed that MZs, determined using EC_a, could be used to characterise spatial variation in skeleton vineyards. However, to our knowledge, there is no example using a combined sensor system for delineating management zones. Several methods of data analysis have been developed for determination of these sub-field areas and at present there is no univocally accepted methodology. Geostatistics treats each attribute of spatial variation as a random regionalized variable, varying continuously and its gradual geographical variation is described by a spatial covariance function. The combined use of different geophysical techniques can actually aid us to map soil features unambiguously, obtaining more accurate quantitative information about spatially varying features.

The objective of this study was to define a combined approach of geostatistics and sensor data fusion to delineate homogeneous zones in an agricultural field, using EMI and γ-ray measurements and DGPS height data.

MATERIALS AND METHODS

Study area

The method of multi-sensor data interpretation and integration is demonstrated with data received from a geophysical survey carried out on an 80-ha cropping field in Corrigin, Western Australia. The soils encountered in this field were deep yellow sand (Eutric Regosol), deep pale sand (Ferralic Arenosol), sandy gravel (Ferric Ferralsol), yellow sandy earth (Xanthic Ferralsol), deep sandy duplex (Haplic Lixisol) and shallow sandy duplex (Leptic Lixisol) (Wong et al. 2001). The field was surveyed simultaneously with two EMI sensors (EM31, EM38 Geonics Ltd, Ontario-Canada), a γ-ray spectrometer (Exploranium GR 256 Fugro Instruments) and a DGPS to determine the geographical locations and elevation with a differential correction, mounted on a vehicle and towed. The survey was carried out on a 30-m line spacing.

Electromagnetic Induction (EMI)

EMI soil survey is based on the principle that a transmitter coil in contact with the soil surface produces a primary electromagnetic field which propagates above and below soil. If a conductive medium is present in the soil, the magnetic field induces a time-varying electromotive force, which induces a flow of eddy currents within the conductor. These currents, in turn, generate a secondary magnetic field, 90° out of phase with the primary field, which is recorded by a receiver coil in the EM unit. The receiver also detects the primary field travelling thought the air, so the apparent conductivity near the receiver is determined by the ratio of the magnitudes of the secondary to primary magnetic field (McNeill, 1980). The instrumentation was an EM31 that has an intercoil spacing of 3.7 meters, which yields an effective depth of exploration of about 6 meters, an EM38 has an intecoil spacing of 1 metre and allows measuring bulk electrical conductivity (EC_a) within an effective depth of 1.5 m. both sensors were used in the vertical dipole mode.

Gamma ray spectrometry

Gamma ray spectrometry is a relatively new soil sensing technique that measures gamma ray radiation emitted from the natural decay of radioactive isotopes that are present in all soils (Cook et al., 1996). There are many naturally occurring elements that have radioactive isotopes, but only potassium (K), uranium (U) and thorium (Th) decay series have radioisotopes (and associated daughter products) that produce gamma rays of sufficient energy and intensity to be measured by gamma ray spectrometry. The source intensity and the source-detector geometry affect observed gamma ray flounce rates. The basis of γ -ray spectrometry is that γ -ray photons have discrete energies, which are characteristic of the radioactive isotopes from which they originate (IAEA, 2003). By measuring the energies of γ -ray photons, it is possible to determine the source of the radiation. Gamma-ray spectrometers typically measure 256 channels that comprise an energy spectrum ranging from 0 to 3 MeV. Radiation not originating from the earth's surface is regarded as background and is removed during data processing. The main sources of background radiation are atmospheric radon (222Rn), cosmic sources and instrumental sources (IAEA, 2003). The γ-ray emission survey was carried out with an

Exploranium γ-ray spectrometer with a thallium-activated sodium iodide crystal scintillation detector. The γ-ray spectra were resolved into individual emissions from potassium, thorium, and uranium according to their characteristic peaks.

Geostatistical Procedures

Firstly, the whole data set was split into four similar groups of variables: 1) EMI data; 2) K counts; 3) Th, U, Tc counts and 4) DGPS height. Geostatistical procedures were separately applied to each group.

MultiGaussian approach

Even if ordinary cokriging does not require the data to follow a normal distribution, variogram modelling is sensitive to strong departures from normality, because a few exceptionally large values may contribute to many very large squared differences. To avoid this problem, a multiGaussian approach was used to produce the maps of the variables. It consists of the following steps:

- a Gaussian transformation of the initial attributes into a Gaussian-shaped variables with zero mean and unit variance. This procedure is known as Gaussian anamorphosis (Chilès and Delfiner, 1999; Wackernagel, 2003) and consists in determining a mathematical function which transforms a variable with a standardised Gaussian distribution into a new variable with any distribution.
- modelling the coregionalization of the set of variables, using the so called Linear Model of Coregionalization (LMC). The LMC, developed by Journel and Huijbregts (1978), considers all the studied variables as the result of the same independent physical processes, acting at N_s spatial scales. The simple and cross variograms of the variables are all modelled by a linear combination of N_s standardized variograms to unit sill (Castrignanò et al., 2000). Fitting of LMC is performed by weighted least-squares approximation under the constraint of positive semi-definiteness of the matrix of sills (coregionalization matrix) corresponding to each spatial scale, using an iterative procedure (Lajaunie et al., 1989).

The transformed data are then estimated at all unsampled locations using ordinary cokriging (Goovaerts, 1997). Finally, the estimates are back transformed to the raw data through the mathematical model calculated in Gaussian Anamorphosis. For those variables which do not show a strong correlation with other variables a univariate approach is preferred by variogram fitting and kriging.

Intrinsic random functions of order k (IRF-k)

As the elevation data recorded by DGPS showed a trend, they were interpolated using intrinsic random functions of order k (IRF-k) technique of non stationary geostatistics. The theory of IRF-k was formulated by Matheron (1973) for linear geostatistical analysis and defines an IRF-k as a random function with stationary increments of order k. In IRF-k kriging, the structural analysis is done in two steps: first the order, k, of the drift expressed as a polynomial, is established, and secondly the generalized covariance, K(h), of the distance, h, is calculated and a parametric model is then fitted to it. To determine the degree of drift the least-squares errors are ranked in ascending magnitude for each polynomial order of k =0, 1 or 2. The first rank is assigned to the order producing the

smallest error, the second rank to the second one, and so on. These ranks are finally averaged for each target point and the smallest averaged rank corresponds to the optimal degree of the drift. Cross validation is used to select the optimal generalized covariance; the model that leads to a standardized error closest to 1 is retained (Buttafuoco et al., 2005).

All statistical and geostatistical analyses were done by using the software package ISATIS®, release 9.06 (Geovariances, 2009).

Visualising MZ delineation using RGB colour triplet

A statistical colouring scheme (Hargrove and Hoffman, 2005) is used to visualise soil similarities within different MZs. PCA is applied before clustering to condense a larger number of "raw" variables into orthogonal principal component axes and the top three PCA components are mapped with a red-green-blue (RGB) colour triplet. The unique colour of each MZ is derived by a mixture of RGB weighted by relative contribution of each of the three components to each MZ, so reflecting the degree of similarity among MZs.

RESULTS AND DISCUSSION

The descriptive statistics of the sensor data from the very dense sampling points are summarised in Table 1, after removing data outliers (points outside ± 2.5 standard deviations from the field average). It is evident that the soil is generally characterised by large variability and the distributions look strongly positively skewned, with the exception of elevation, and with sensible departures from normal distribution. Therefore, we preferred to normalise and standardise all data to mean 0 and variance 1, by using Hermite polynomial expansions restricted to the 30th order at which the ratio between the variance of the anamorphosis function and the variance computed from the data was approximately constant and equal to one (Wackernagel, 2003).

Table 1. Descriptive statistics of the sensor data.

VARIABLE	Min	Max	Mean	Skewness	Kurtosis	Std. Dev	Variance
Em31(mSm^{-1})	43.3	137.4	61.48	2.604	11.714	12.453	155.079
Em38(mSm^{-1})	0.741	45.629	7.575	3.035	15.11	5.308	28.175
DPGS Height (m)	305.745	326.008	314.4	0.333	2.009	5.265	27.723
γ-K (Counts 100s^{-1})	0.5	104	17.894	2.523	11.399	12.835	164.748
γ-Tc (Counts 100s^{-1})	156	2675.5	515.316	1.962	6.234	474.589	225235.11
γ-Th (Counts 100s^{-1})	7	404	63.986	2.042	6.611	71.918	5172.214
γ-U (Counts 100s^{-1})	6.5	231	44.124	1.95	6.17	40.408	1632.841

Table 2 lists the correlation coefficients of all the variables. The EMI variables were strongly correlated and the four γ variables were correlated as well, however the correlations between γ-K and the other γ variables (γ-U, γ-Th and γ-Tc) were weaker. Poor correlation between EMI and γ-radiometric data may be due to these sensors responding to different soil properties. As regards elevation, it showed no correlation with EMI data, whereas it looked correlated with the γ variables, but at a less extent with K. These preliminary considerations about the different behaviour of the four groups of variables justify carrying out a separate analysis for each group.

Table 2. Correlation matrix for geophysical measurements across the study filed. Correlation coefficient >0.13 is significant at 0.05 probability level.

VARIABLE	Em31	Em38	Height	γ-K	γ-Tc	γ-Th	γ-U
Em31	1						
Em38	0.868	1					
Height	-0.1	-0.076	1				
γ-K	-0.078	-0.035	0.373	1			
γ-Tc	-0.033	-0.041	0.571	0.66	1		
γ-Th	-0.032	-0.045	0.566	0.623	0.997	1	
γ-U	-0.027	-0.036	0.572	0.62	0.997	0.995	1

DGPS height showed a quite evident anisotropy along the 20°N direction and the variable was not stationary, as results from its directional variogram (not reported). Therefore, a non-stationary approach was applied. For drift identification, 10 trend models were compared consisting of different combinations of linear and quadratic components of coordinates. The model which realised the minimum rank error was a combination of all components, both linear and quadratic of the coordinates. After filtering drift, the stochastic component of variation was estimated by a linear function of the generalised covariance with the scale parameter equal to 147.87 m and the sill to 0.011.

The map of DGPS height shows a clear increasing trend in NW-SE direction. The field slopes down from a ridge that is oriented in the NE direction to a valley bottom that is oriented in approximately the same direction (Figure 2a). The soil map of the field (Figure 2b), based on a pedological understanding of this landscape and soil profile observations, is reproduced here from Wong et al., 2001. The top of the ridge is dominated with a sandy gravel soil and the heaviest topsoil for this field (yellow sandy earth) is associated with this ridge. The lowest part of the field contains duplex soils characterised by a sharp texture contrast from sandy topsoil to clayey subsoil down the profile. The depth to texture contrast becomes shallower to the west of the field and the shallowest area is not cropped. This low lying area of duplex soils impedes drainage and is subject to intermittent water logging and is prone to salinity due to raising saline water table. Deep sands extend from the sides of the deep duplex soils.

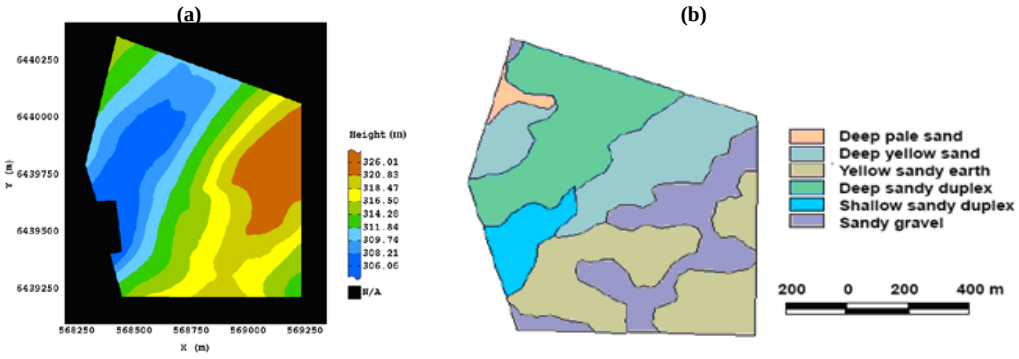

Figure 2. Spatial estimate of DGPS height (a) (Color scale uses isofrequency classes). Soil map reproduced from Wong et al., 2001 (b).

The directional EMI variograms showed a clear zonal anisotropy along the 40°N direction (not shown), therefore an anisotropic Linear Model of Coregionalization (LMC)

was fitted to the variograms of the Gaussian variables of EM31 and EM38. LMC includes four basic structures: 1) a nugget effect; 2) an isotropic spherical model with range= 100.00 m; a zonal anisotropic spherical model along the direction of larger spatial continuity N40° with range=400 m and 4) a zonal anisotropic spherical model along the N130° direction with range=300 m (Table 3). The appropriateness of the LMC was evaluated with a cross-validation test by calculating mean error and the variance of standardised error, which were quite close to 0 and 1. From the cumulative values of the eigenvalues associated to each spatial structure it results that the main components of variation are along the two directions of zonal anisotropy.

Table 3. Linear Model of Coregionalization (LMC) for the variograms of the Gaussian variables of EM31 and EM38

Nugget effect (Cumulative Eigenvalue=0.0581)

	g*EM31	gEM38
gEM31	0.0085	-0.0205
gEM38	-0.0205	0.0496

Isotropic Spherical Model (Range = 100 m; Cumulative Eigenvalue=0.4341)

	gEM31	gEM38
gEM31	0.2345	0.1969
gEM38	0.1969	0.1997

Anisotropic Spherical Model (N40° Range=400m; Cumulative Eigenvalue=1.7286)

	gEM31	gEM38
gEM31	0.8419	0.6432
gEM38	0.6432	0.8867

Anisotropic Spherical Model (N130° Range=300m; Cumulative Eigenvalue=1.8244)

	gEM31	gEM38
gEM31	0.8658	0.7376
gEM38	0.7376	0.9586

* g means Gaussian transformed variable

The EM31 and EM38 maps have the same main patterns of spatial dependence and look quite similar (Figures 3 a-b). However, the EM31 values were generally greater than EM38 due to deeper depth of soil sensing and differences in subsoil. High EMI values occurred on low-lying duplex soils due to tendency for water accumulation, salinisation and occurrence of subsoil clay. High EMI values could not discriminate these valley bottom soils from areas of yellow sandy earth found on the hill. Similarly, low EMI values cannot be used on their own to identify areas of deep sands from sandy gravelly soils as both sand and gravel retain little water and have low electrical conductivities.

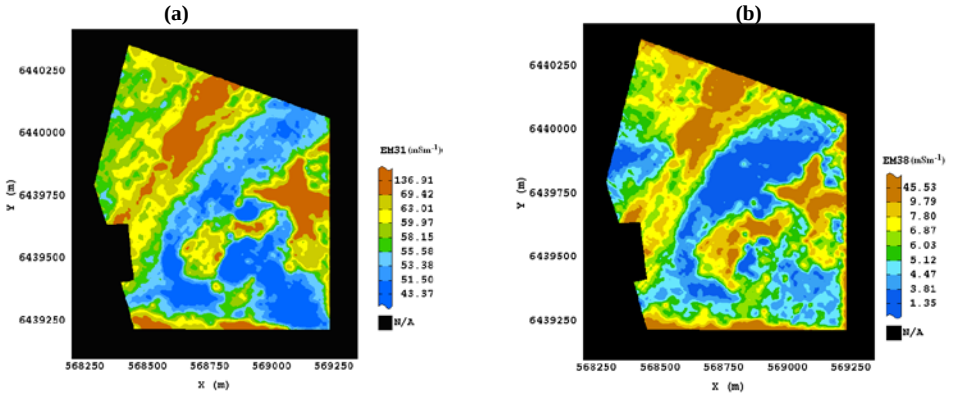

Figure 3. Spatial estimates of apparent soil electrical conductivity measured by EM31(a) and EM38 (b). (Color scale uses isofrequency classes).

Gamma-radiometric counts from K directional variogram showed a zonal anisotropy along E-W direction (not showed), therefore an anisotropic variogram was fitted with approximately the same basic structures as reported for EMI data but with different directions of anisotropy (Table 4).

Table 4. Directional variogram model of g γ-K

Nugget effect
Sill = 0.194
Isotropic Spherical Model (Range = 100 m)
Sill = 0.008
Anisotropic Spherical Model (N90° Range = 450 m)
Sill = 0.823
Anisotropic Spherical Model (N0° Range = 400 m)
Sill = 1.058

The kriged map of K shows a well defined structure, characterised by the higher values at the top of the field (Figure 4a) but swung 50° to E with respect the direction of the valley bottom. In contrast, the variables γ-U, γ-Th and γ-Tc showed a geometric anisotropy with the longer range along the 30oN direction (directional variograms not reported). This means that they mostly respond to the same process acting on the whole area but with different gradients depending on direction. An anisotropic geometric LMC, with the direction of larger spatial continuity along the N30° direction, was fitted to the variograms of the three Gaussian γ variables, including three basic structures: a nugget effect; an isotropic spherical model with range =100 m and a geometric anisotropic spherical model with range= 500 m (Table 5). As for EMI data, most variation was directional. The maps of the three variables (Figures 5b, c, d) look quite similar, due to the strong correlations between these variables, with a common structure characterised by the higher values in the elevated part of the field.

Table 5. LMC of the Gaussian γ variables

Nugget effect (Cumulative Eigenvalue=0.0509)

	g γ-Tc	g γ-Th	g γ-U
g γ-Tc	0.009	-0.0055	-0.0064
g γ-Th	-0.0055	0.0074	-0.0072
g γ-U	-0.0064	-0.0072	0.0345

Isotropic Spherical Model (Range=100 m) Cumulative Eigenvalue=0.0798)

	g γ-Tc	g γ-Th	g γ-U
g γ-Tc	0.0158	-0.0151	0.0088
g γ-Th	-0.0151	0.0183	-0.0211
g γ-U	0.0088	-0.0211	0.0457

Geometrical Spherical Model (N30° Range=600 m, N120° Range=500m, Cumulative Eigenvalue=3.6064)

	g γ-Tc	g γ-Th	g γ-U
g γ-Tc	1.2277	1.2141	1.2026
g γ-Th	1.2141	1.2007	1.1893
g γ-U	1.2026	1.1893	1.178

All of the four γ maps mostly show the same main patterns of spatial dependence, even if the map of γ-K differ somewhat from the other γ-radiometric maps. In contrast the EMI maps show a characteristic banding of low alternating to high values of bulk ECa parallel to the direction of the valley bottom. The above results provide some considerations about the strength and weakness of each individual sensor.

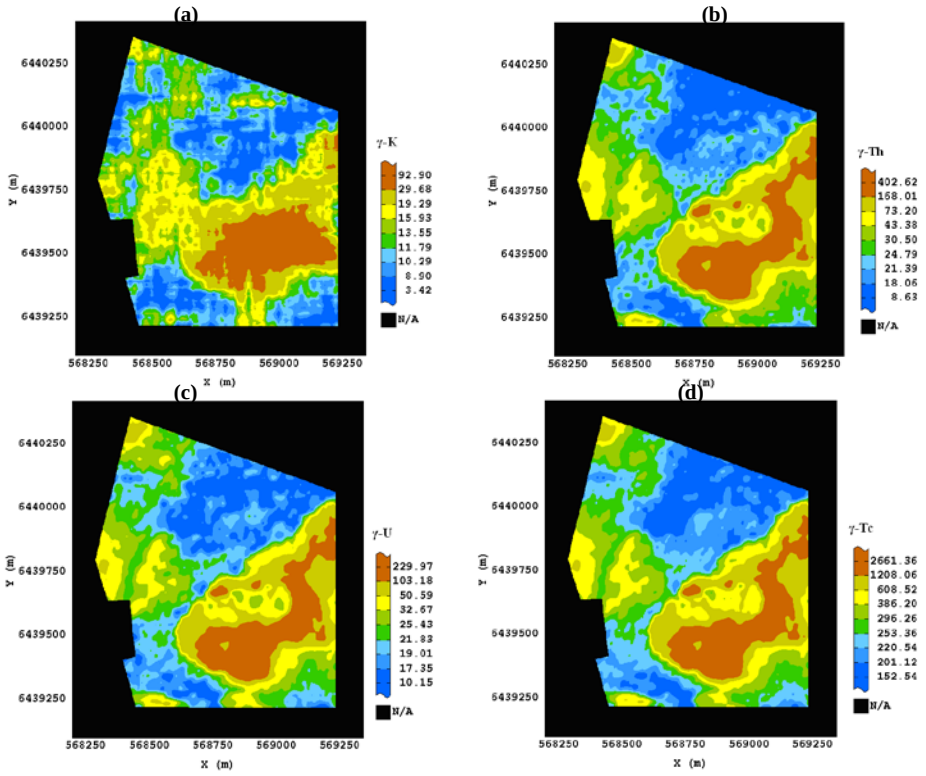

Figure 4. Spatial estimates of gamma-ray emission from potassium (K) (a), thorium (Th) (b), uranium (U) (c) and total emission (Tc) (d). (Color scale uses isofrequency classes).

Areas with high EMI values can be resolved into (1) the low-laying duplex soil where γ-radiometric values are in contrast low and (2) areas of heavier textured yellow sandy earth found where γ-radiometric values are also high (Figures 3 and 4). Areas with low EMI values can also be resolved into (1) areas of deep sands where γ-radiometric values are also low and (2) areas of sandy gravels where γ-radiometric values are high. Thus only the use of a multi-sensor platform can discriminate soils that give similar outputs to one sensor.

To synthesise the complex multivariate spatial variation of the field in a restricted number of zones to be submitted to the same management, the traditional Principal Component Analysis was applied to the data set including the estimates of the seven variables. Since each eigenvalue is proportional to the variance associated with the corresponding principal component (PC) and the variables were standardised to unit variance, we retained only the eigenvectors producing eigenvalues greater than one. Therefore, we focused on the first two PCs, which account for about 58% and 27% of the total spatial variation and cumulatively for more than 85% (Table 6). The loading values for the first PC indicate the γ variables and to a smaller extent elevation but at a less extent, as the most influencing variables, even if they weigh negatively. In contrast, the EMI variables do not affect the first PC significantly. The role of the variables is completely inverted in the second PC, where the EMI variables produce large positive loading values, whereas the influence of the remaining variables is not significant. These results point out what we observed above, the statistical orthogonality among the EMI variables and the topographical and γ variables. Therefore, we expect the maps of the two PCs (Figures 5 a-b) to give us complementary information about the soil properties: the map of the first PC (Figure 5a) looks quite similar, but inverted, respect the γ-U, γ-Th and γ-Tc maps, due to the negative weighting of these variables. The scores of the first PC produce splitting the field into two main zones, located at different elevation and characterised with different pedology: sandy soils at the bottom and sandy earth and sandy gravel at the top. The map of the second PC (Figure 5b), as expected, reproduces the same main structures of spatial dependence of the EMI maps (Figures 3 a-b) and, used together with the previous map, aids us in further partitioning the top of the field into zones at different texture and in ranking the valley bottom at salinity hazard.

Figure 5c shows the delineation in MZs using only the tones of red and green of the RGB-colour triplet to display the first two PCs. Based on the PCs' loadings (table 6), red colours represent low values of γ data and green colours represent high values of EMI data. In this representation individual MZ borders disappear and the colours reveal similarities among the soils in each MZ. Four main colours prevail in the map: 1) a narrow white zone corresponding to the valley bottom, characterised by low γ values and high EMI values (saline sandy soils); 2) a wide red area where sandy soils prevail (low EMI value); 3) a green area characterised by high EMI values (heavier soils) mixed with 4) black areas of small extension, corresponding to high γ values but low EMI value (sandy gravel). This last portion of the field looks quite fuzzy, without abrupt colour changes but with subtle colour changes following the meandering contours of the transition areas.

A combined use of different geophysical devices could then be used to estimate the plant-available water storage capacity of the soil and identify areas with the highest yield potential as well as limiting factors such as high salt levels or subsoil constraints.

However, since electromagnetic sensing and gamma spectrometry depend on many factors, caution should be used in the interpretation of data. Yield maps over several years are likely to mirror the spatial distribution of the soil constraints. Therefore yield maps, maps of soil type and multi-geophysical sensing could be jointly interpreted by the agronomist in collaboration with the farmer to help him make better management decisions and reduce input costs.

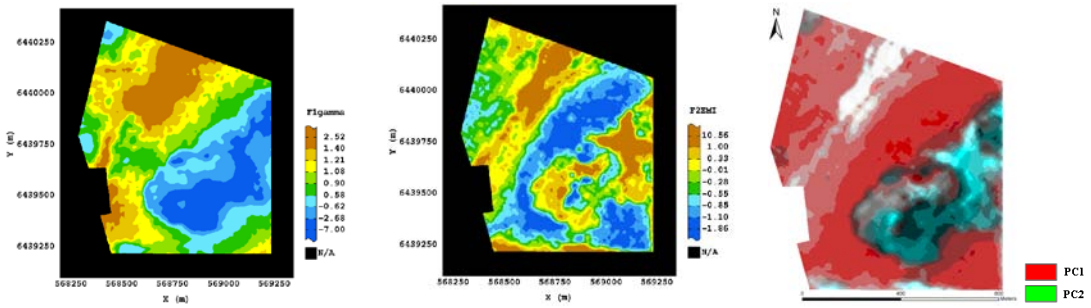

Figure 5. Spatial distribution of first (a)and second (b)principal components and RGB map of the first two PCs (c).

Table 6. Loading coefficients of the first two PCs.

	EM31	EM38	DGPS Height	K	Tc	Th	U	Eigen Val.	Variance %
PC 1	0.0471	0.0405	-0.3203	-0.4217	-0.4898	-0.4872	-0.4883	4.0557	57.94
PC 2	0.6989	0.7008	-0.0972	0.0777	0.0399	0.0391	0.0431	1.9179	27.4

CONCLUSION Management decisions, such as subsoil amelioration and variable rate fertiliser, lime and irrigation application, require knowledge of the soil properties and where subsoil constraints may occur across the field, so limiting root growth and crop development. Yield, EMI and gamma-ray emission mapping, together with the farmers' knowledge, may provide an opportunity to locate the subsoil constraints.

However, commonly used EMI sensors have often failed to distinguish between major contrasting soils typically encountered across a field. This problem can be solved by using multiple-sensors, each with strengths that compensate for the weaknesses of the other sensors. The outputs of these sensors can be integrated efficiently using geostatistical techniques and traditional principal component analysis and sometimes few principal components are sufficient to describe the variation of soil at the spatial resolution matching that of yield maps.

Research in Precision Agriculture has focused on dividing a field into few relatively uniform management zones as a practical and cost-effective approach for variable application of water and chemical inputs. In this study EMI, γ-ray and DGPS sensors were used to delineate agricultural management zones, characterised by differences in physical, chemical, textural and topographical properties, which might potentially have an impact on crop yield. However, as spatial and temporal variability in crop response

depends on many factors, including weather, genetics, soil and landscape properties, management practices, stresses, pests and their dynamic interactions, it is advised to jointly use any other piece of information, for example derived from crop simulation or farmers' knowledge. Moreover, the static concept of MZ can be inadequate for variable application of crop inputs as water or fertilizer under variable meteorological conditions. Crop simulation is advisable to integrate the soil, crop and weather data to aid management of these zones. Another strategy might be to combine proximal geophysical surveys of crop fields with remote imaging, so that crop status can be instantaneously estimated and then better management decisions can be made.

Acknowledgements We are grateful to the Australian Grains Research and Development Corporation (GRDC) for funding the field research reported here. Collaborative work between MW and AMC was funded by the Australian Academy of Science under its Scientific Visit to Europe Program. We are grateful to the CRA for hosting this work.

REFERENCES

Buttafuoco, G. and Castrignanò, A., 2005. Study of the spatio-temporal variation of soil moisture under forest using intrinsic random functions of order k. Geoderma, 128, 208-220.

Castrignanò, A., Giugliarini, L., Risaliti, R., Martinelli, N., 2000. Study of spatial relationships among some soil physico-chemical properties of a field in central Italy using multivariate geostatistics. Geoderma, 97, 39–60.

Castrignanò, A., Morari, F., Morelli, G., 2006. Assessment of spatial relationship between some soil properties and electromagnetic induction scans. Agricultural Engineering For a Better World. XVI CIGR World Congress, 1-6.

Chilès, J. P. and Delfiner, P., 1999. Geostatistics: Modeling Spatial Uncertainty, Wiley & Sons, New York.

Cook, S.E., Corner R.J., Groves P.R., Grealish G.J., 2006. Use of airborne gamma radiometric data for soil mapping. Australian Journal of Soil Research, 34, 1, 183 – 194.

Corwin, D.L. and Lesch, S.M., 2003. Application of soil electrical conductivity to precision agriculture: Theory, principles, and guidelines, Agronomy Journal., 95: 455-471.

Doolittle, J.A., Sudduth, K.A., Kitchen, N.R., Indorante, S.J., 1994. Estimating depths to claypans using electromagnetic induction methods. Journal of Soil and Water Conservation 49, 572–575.

Géovariances, 2009. Isatis Technical Ref., ver. 9.06 Geovariances & Ecole Des Mines De Paris: Avon Cedex, France.

Goovaerts, P. 1997. Geostatistics for natural resources evaluation. Oxford University Press, New York.

Hargrove W.W., Hoffman F.M, 2005. Potential of multivariate quantitative method for delineation and visualization of ecoregions. Environmental Management, 34, suppl. 1: S39-S60.

International Atomic Energy Agency, IAEA, 2003. Guidelines for Radioelement Mapping Using Gamma Ray Spectrometry Data. IAEATECDOC-1363. IAEA, Vienna.

Kaffka, S.R., Lesch, S.M., Bali, K.M., and Corwin, D.L., 2005. relationship of

electromagnetic induction measurements, soil properties, and sugar beet yield in salt-affected fields for site-specific management. Computer and Electronics in Agriculture, 46, 329-350.
Kitchen, N. R., Drummond, S. T., Lund, E. D., Sudduth, K. A., Buchleiter, G. W., 2003. Soil Electrical Conductivity and Topography Related to Yield for Three Contrasting Soil–Crop Systems. Agronomy Journal 95, 483-495.
Journel, A.G. and Huijbregts, C.J., 1978. Mining Geostatistics. Academic Press: New York.
Lajaunie, C. and Béhaxétéguy, J.P. Elaboration d'un programme d'ajustement semi-automatique d'un modèle de corégionalisation – Theorie. technical report N21/89/G. Paris: ENSMP, 1989, 6p.
Lark, R.M., 1998. Forming spatially coherent regions by classification of multi-variate data: an example from the analysis of maps of crop yield. International Journal Geographical Information Science 12, 1, 83-98.
Matheron G., 1973. The intrinsic random functions and their applications. Advances in Applied Probability, 5, 239-465.
McBratney, A.B., Minasny, B., Whelan, B.M., 2005. Obtaining 'useful' high-resolution soil data from proximally-sensed electrical conductivity/resistivity (PSEC/R) surveys. In: Stafford, J.V. (ed.), Precision Agriculture '05, Proceedings of the 5th European Conference on Precision Agriculture. Wageningen Academic Publishers, The Netherlands, 503–510.
McNeill J.D., 1980. Electromagnetic terrain conductivity measurement at low induction numbers. Geonics Limited, Technical Note TN 6. Geonics Ltd. Mississauga, Ontario, Canada.
Morari, F., Castrignanò, A., Pagliarin, C., 2009. Application of multivariate geostatistics in delineating management zones within a gravelly vineyard using geo-electrical sensors. Computers and Electronics in Agriculture 68, 97–107.
Viscarra Rossel, R.A., Taylor, H.J., McBratney, A.B., 2007. Multivariate calibration of hyperspectral γ-ray energy spectra for proximal soil sensing. European Journal of Soil Science 58, 343–353.
Wackernagel, H., 2003. Multivariate Geostatistics: an introduction with Applications. Springer Verlag, Berlin, 3rd ed., pp. 388.
Wong, M. T. F., R. J. Corner, and S. E. Cook. 2001. A decision support system for mapping the site-specific potassium requirement of wheat in the field. Australian Journal of Experimental Agriculture 41, 655–661.
Wong, M.T.F., Asseng, S., 2006. Determining the causes of spatial and temporal variability of wheat yields at sub-field scale using a new method of upscaling a crop model. Plant and Soil 283, 203–215.
Wong, M.T.F., Asseng, S., Zhang, H., 2006. A flexible approach to managing variability in grain yield and nitrate leaching at within-field to farm scales. Precision Agriculture 7, 405–417.
Wong, M.T.F., Asseng, S., Robertson, M.J., Oliver, Y., 2008. Mapping subsoil acidity and shallow soil across a field with information from yield maps, geophysical sensing and the grower. Precision Agriculture 9, 3–15.
Wong, M.T.F., Oliver, Y.M., Robertson, M.J., 2009. Gamma-radiometric assessment of soil depth across a landscape not measurable using electromagnetic surveys. Soil Science Society of America Journal, 73, 1261-1267.